Int. J. Electrochem. Sci., 13 **(2018)** 2498 – 2508, doi: 10.20964/2018.03.72

International Journal of
ELECTROCHEMICAL
SCIENCE
www.electrochemsci.org

Dehydration of $FePO_4 \cdot 2H_2O$ for the Synthesis of $LiFePO_4$/C: Effect of Dehydration Temperature

Wuliang Gongyan[1,2,3], *Lingmeng Li*[1,2,3], *Haisheng Fang*[1,2,3,*]

[1] Key Laboratory of Advanced Battery Materials of Yunnan Province, Kunming University of Science and Technology, Kunming 650093, China
[2] Key Laboratory of Nonferrous Metals Vacuum Metallurgy of Yunnan Province, Kunming University of Science and Technology, Kunming 650093, China
[3] Faculty of Metallurgy and Energy Engineering, Kunming University of Science and Technology, Kunming 650093, China
[*]E-mail: hsfang1981@hotmail.com

Received: 12 November 2017 / *Accepted:* 12 January 2018 / *Published:* 5 February 2018

To study the effect of dehydration temperature on synthesis and electrochemical performance of $LiFePO_4$/C, $FePO_4 \cdot 2H_2O$ is dehydrated at different temperatures (200-700 ^oC) and the resulting $FePO_4$ is adopted as a raw material to synthesize $LiFePO_4$/C composite. The results show that $FePO_4 \cdot 2H_2O$ can be fully dehydrated at a temperature above 184 ^oC, the crystalline form, particle size and morphology of the dehydrated $FePO_4$ varies with dehydration temperature, and the synthesized $LiFePO_4$/C composites from these $FePO_4$ have similar crystallinity, particle size and morphology, but have different electrochemical performance. Among all samples, the $LiFePO_4$/C synthesized from the $FePO_4$ dehydrated at 500 ^oC exhibits the best electrochemical performance. From these results, it is suggested that α-quartz $FePO_4$ with a trigonal structure ($P3_121$) is an optimum form for efficient synthesis of high performance $LiFePO_4$/C composite, and the dehydration of $FePO_4 \cdot 2H_2O$ should be controlled at a temperature around 500 ^oC.

Keywords: Lithium ion batteries; Cathode materials; $LiFePO_4$; $FePO_4 \cdot 2H_2O$; Dehydration

1. INTRODUCTION

Olivine-structured $LiFePO_4$ has been widely used as a commercial cathode material for lithium ion batteries, and carbon coating is required for its practical application due to its extremely low electronic and ionic conductivity [1]. Now, commercial $LiFePO_4$/C composite is mainly produced via a solid state method by sintering the solid mixture of iron source, lithium source, phosphorus source and carbon source. Among these raw materials, the iron source is the most critical one and can be divided

into two types: ferrous iron source [2-5] (ferrous oxalate) and ferric iron source [6-8] (including ferric phosphate and ferric oxide). At present, ferric phosphate has become the first choice as an iron source (also as a phosphorus source) for industrial production of $LiFePO_4$/C composite based on a carbothermal reduction method. Ferric phosphate can exist in a hydrated form ($FePO_4 \cdot xH_2O$) [9,10,12,14-15] and anhydrous form ($FePO_4$), and the anhydrous $FePO_4$ is preferred for industrial production of $LiFePO_4$/C composite [16-19]. In general, anhydrous $FePO_4$ is produced by dehydration of $FePO_4 \cdot xH_2O$, and different crystalline forms of $FePO_4$ can be yielded upon dehydration temperature [9,12,15]. The dehydrated $FePO_4$ may exists in a single form such as orthorhombic strengite (*Pbca*), monoclinic phosphosiderite ($P2_1/n$), trigonal α-quartz ($P3_121$) or in a mixed state of these forms [9,15]. Generally, these forms of $FePO_4$ can all be used to synthesize $LiFePO_4$/C composite, but it is still not yet certain whether the crystalline form of $FePO_4$ has an influence on the synthesis and electrochemical performance of $LiFePO_4$/C composite. Meanwhile, the particle size of dehydrated $FePO_4$ is also upon dehydration temperature, and a high-temperature dehydration may give rise to undesirable particle growth. Since reducing particle size is highly beneficial to the electrochemical performance of $LiFePO_4$ [20], it is best to avoid undesirable particle growth of dehydrated $FePO_4$. Therefore, the effect of dehydration temperature should be well studied and the dehydration of $FePO_4 \cdot 2H_2O$ should be deliberately considered.

In this paper, the thermal evolution of $FePO_4 \cdot 2H_2O$ dehydration is studied and different forms of anhydrous $FePO_4$ obtained at different dehydration temperatures are adopted to synthesize $LiFePO_4$/C whose electrochemical performance is evaluated and compared.

2. METHODS

A certain amount of $FePO_4 \cdot 2H_2O$ was transferred to a muffle furnace and heated at a set temperature (200, 300, 400, 450, 500, 600 or 700 ^oC) for 2 h in air. The heating rate is 2 $^oC\ min^{-1}$. Anhydrous $FePO_4$ powders were obtained after furnace cooling to room temperature.

Stoichiometric amounts of anhydrous $FePO_4$ obtained at different dehydration temperatures and Li_2CO_3 were ball-milled with sucrose (8 wt. % of $LiFePO_4$) in 40 ml de-ionized water for 4 h. The mixed slurry was dried and then transferred to a box furnace and sintered (heating rate 2 $^oC\ min^{-1}$) at 700 ^oC for 10 h in argon atmosphere to synthesize $LiFePO_4$/C powders. The resulting products were defined as S200, S300, S400, S450, S500, S600 and S700, respectively. To reduce particle size of $LiFePO_4$/C further, additional synthesis experiment was implemented for the $FePO_4$ dehydrated at 500 ^oC. We decreased the de-ionized water to 28 mL (liquid/solid ratio: 0.5) and extended ball milling time to 6 h for raw materials mixing while other processing conditions were kept. The resulting product was defined as S500'.

The crystalline phase of the obtained materials was identified by X-ray diffraction (XRD, D/MaX-3B, Rigaku). Thermogravimetric and differential thermal analysis (TG/DTA) was performed with a thermal analysis instrument (Mettler Company HT/1600) from room temperature to 700 ^oC at a heating rate of 2 $^oC\ min^{-1}$ in a constant flow of extra dry air. The particle size and morphology of $FePO_4$ and $LiFePO_4$ was observed by scanning electron microscopy (SEM, Quanta250, FEI

Company). The amount of residual carbon in the composite was determined by C-S analyzer (Corey-150C, Corey Company).

Electrochemical performance of samples was evaluated using CR2025 coin cells with a lithium metal anode. The electrolyte was 1 M $LiPF_6$ in EC/DMC (1:1 in volume) solution. The cathode was made by mixing $LiFePO_4$/C, C (super P) and polyvinylidene fluoride (PVDF) with a weight ratio of 8:1:1 in N-methyl- pyrrolidinone (NMP) to form homogenous slurry. Then the slurry was coated on an aluminum foil and dried. The obtained cathode with a diameter of 1.3 cm had a typical loading of ~12 mg active material. All cells were assembled in an argon-filled glove box. Charge/discharge test was performed between 2.5 and 4.0 V at 30 ^oC using Land CT2001A test system. For cycle test, cells were charged at 0.2 C or 1 C (1 C is equal to 150 mA g^{-1}) to 4.0 V, held at 4.0 V until the current decreased to 0.02 C, and then discharged at 0.2 C or 1 C to 2.5 V. For rate test, cells were charged at 0.2 C to 4.0 V, held at 4.0 V until the current decreased to 0.02 C, and then discharged at various rates (0.2 C, 0.5 C, 1 C, 2 C) to 2.5 V. The capacity was calculated on the mass of $LiFePO_4$/C in the cathode.

3. RESULTS AND DISCUSSION

Three factory samples of $FePO_4 \cdot 2H_2O$ were purchased from three different manufacturers, and XRD measurement revealed that all samples were composed of two crystalline forms of $FePO_4 \cdot 2H_2O$. Fig. 1 presents a typical XRD pattern of one of these $FePO_4 \cdot 2H_2O$ samples. It is clear that the sample is a mixture of two crystalline forms which are corresponding to an orthorhombic structure with a space group of *Pbca* and a monoclinic structure with a space group of $P2_1/n$ [9, 15].

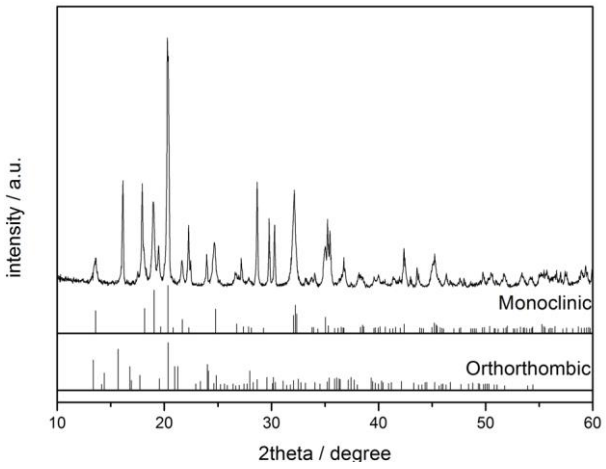

Figure 1. XRD pattern of $FePO_4 \cdot 2H_2O$.

The thermal evolution of $FePO_4 \cdot 2H_2O$ powders was monitored by TG/DTA. As shown in Fig. 2, there is a very sharp endothermic peak at 184 ^oC on the DTA curve together with a rapid weight loss (~ 19 wt. %) on the TG curve, which is related to a quick dehydration of $FePO_4 \cdot 2H_2O$. In the subsequent heating up to 700 ^oC, no significant weight loss is observed on the TG curve, but an

obvious exothermic peak at 632 ^{o}C together with several tiny peaks such as at 440 and 670 ^{o}C are detected in the DTA curve, indicating the occurrence of phase transitions of $FePO_4$ on the heating. The TG/DTA measurement suggests that dehydration of $FePO_4 \cdot 2H_2O$ can be completed at a temperature above 184 ^{o}C and subsequent heating involves phase transitions of $FePO_4$.

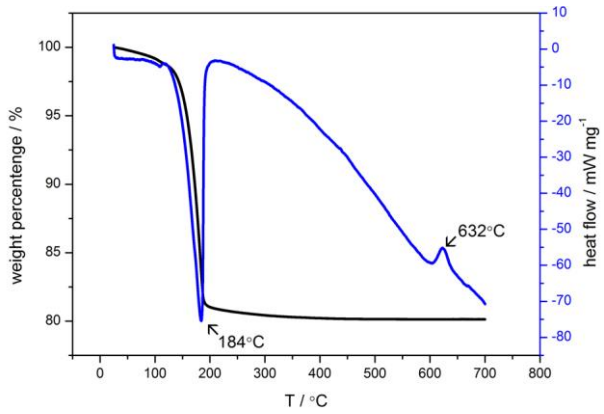

Figure 2. TG/DTA curves of $FePO_4 \cdot 2H_2O$.

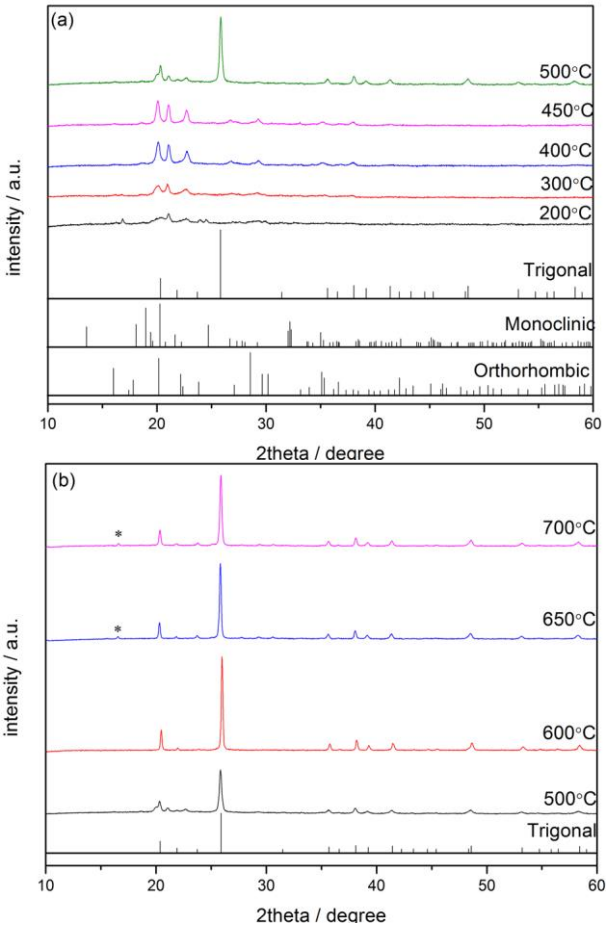

Figure 3. XRD patterns of $FePO_4$ dehydrated at 200-700 ^{o}C.

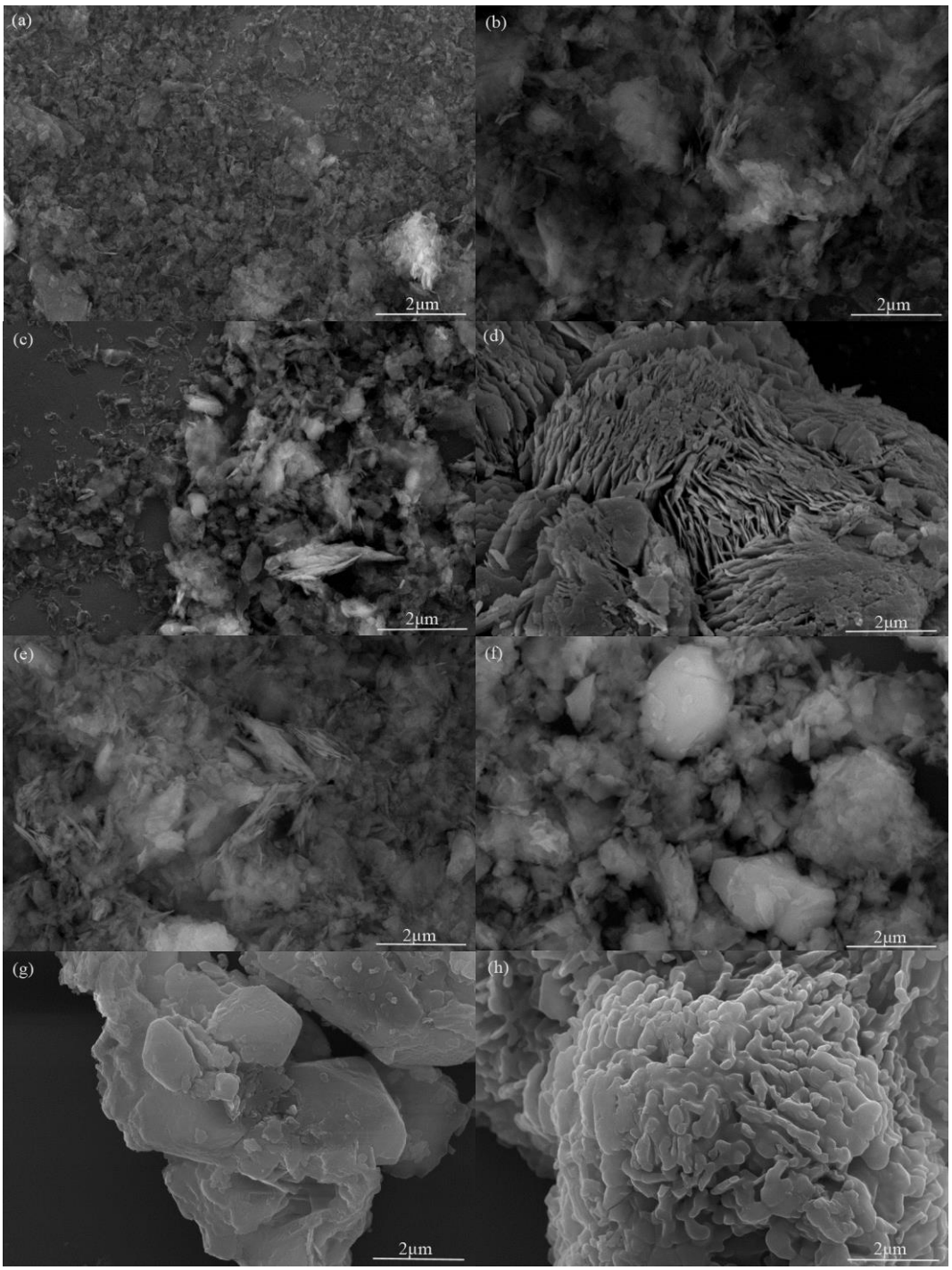

Figure 4. SEM images of (a) $FePO_4 \cdot 2H_2O$ and $FePO_4$ obtained at different dehydration temperatures: (b) 200 ^oC, (c) 300 ^oC, (d) 400 ^oC, (e) 450 ^oC, (f) 500 ^oC, (g) 600 ^oC, (h) 700 ^oC.

Fig. 3 shows XRD patterns of $FePO_4$ obtained at different dehydration temperatures. Clearly, the pattern changes significantly with dehydration temperature. At 200 and 300 ^oC, although the crystal water has already been dehydrated from crystalline structure, dehydration involves only minor rearrangements of the framework and the structure is not destroyed [15]. Therefore, the two samples dehydrated at 200 and 300 ^oC are a mixture of orthorhombic $FePO_4$ (*Pbca*) and monoclinic $FePO_4$ ($P2_1/n$). When the temperature increases to 400 and 450 ^oC, the orthorhombic $FePO_4$ transforms to a

tridymite form of $FePO_4$ with a space group of $P6_3mc$, while the monoclinic $FePO_4$ is stable in this temperature range. Formation of α-quartz $FePO_4$ with a trigonal structure ($P3_121$) is observed at a dehydration temperature of 500 ^oC [21] as highlighted by a new strong diffraction peak at ~26 degree in the pattern, and pure α-quartz phase of $FePO_4$ is obtained at 600 ^oC as shown in Fig. 3b. Further increasing dehydration temperature to 650 and 700 ^oC leads to the appearance of a new diffraction peak (indicated by asterisk in Fig.3b) which may be associated with the formation of an intermediate phase between α phase and β phase of $FePO_4$ [22]. This phase transition can be correlated to the exothermic peak of 632 ^oC observed in the TGA curve (Fig. 2).

Fig. 4 shows SEM images of $FePO_4 \cdot 2H_2O$ and $FePO_4$ obtained at different dehydration temperatures. Apparently, the particle size and morphology of $FePO_4$ is also highly affected by dehydration temperature. As shown in Fig. 4, $FePO_4 \cdot 2H_2O$ and $FePO_4$ obtained at dehydration temperatures below 500 ^oC have a similar morphology which is composed of aggregates of flakes. As the dehydration temperature increases up to 500 ^oC, it seems that the flakes in some aggregates begin to fuse together and a few big crystals are observed in Fig. 4f. Further increasing dehydration temperature to 600 ^oC results in an undesirable particle growth, and all aggregates of flakes are fused into big crystals (Fig. 4g). Similar behavior was also observed in the previous literature [13]. However, a large number of new small crystals appear on the surface of $FePO_4$ crystals at the dehydration temperature of 700 ^oC, which should be connected to the precipitation of an intermediate phase between α phase and β phase of $FePO_4$ caused by the phase transition at ~632 ^oC as observed by TG/TGA (Fig. 2) and XRD (Fig. 3b).

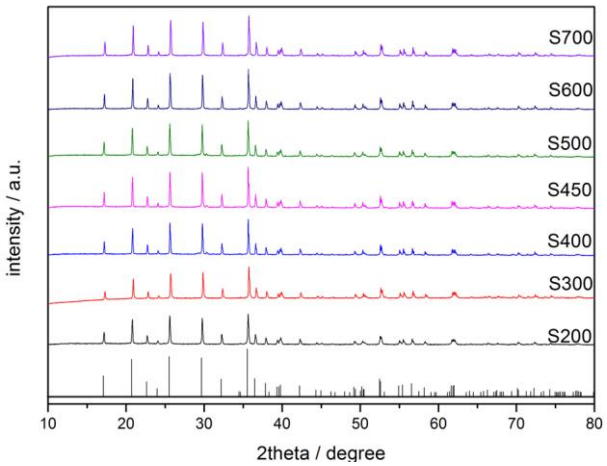

Figure 5. XRD patterns of $LiFePO_4$/C synthesized from $FePO_4$ obtained at different dehydration temperatures.

The above measurements clearly show that dehydration temperature has a big influence on the crystalline structure, particle size and morphology of the dehydrated $FePO_4$. As a raw material, samples of $FePO_4$ obtained at different dehydration temperatures were adopted to synthesize $LiFePO_4$/C, and the effect of dehydration temperature on $LiFePO_4$/C was evaluated. Fig. 5 shows XRD patterns of the obtained $LiFePO_4$/C. All samples can be indexed into an orthorhombic structure of

$LiFePO_4$ with a space group of *Pnma*. No diffraction peaks of carbon is observed in all patterns indicating the amorphous state of the residual carbon in the synthesized composites, and the carbon content of all samples is around 3.2 wt. %.

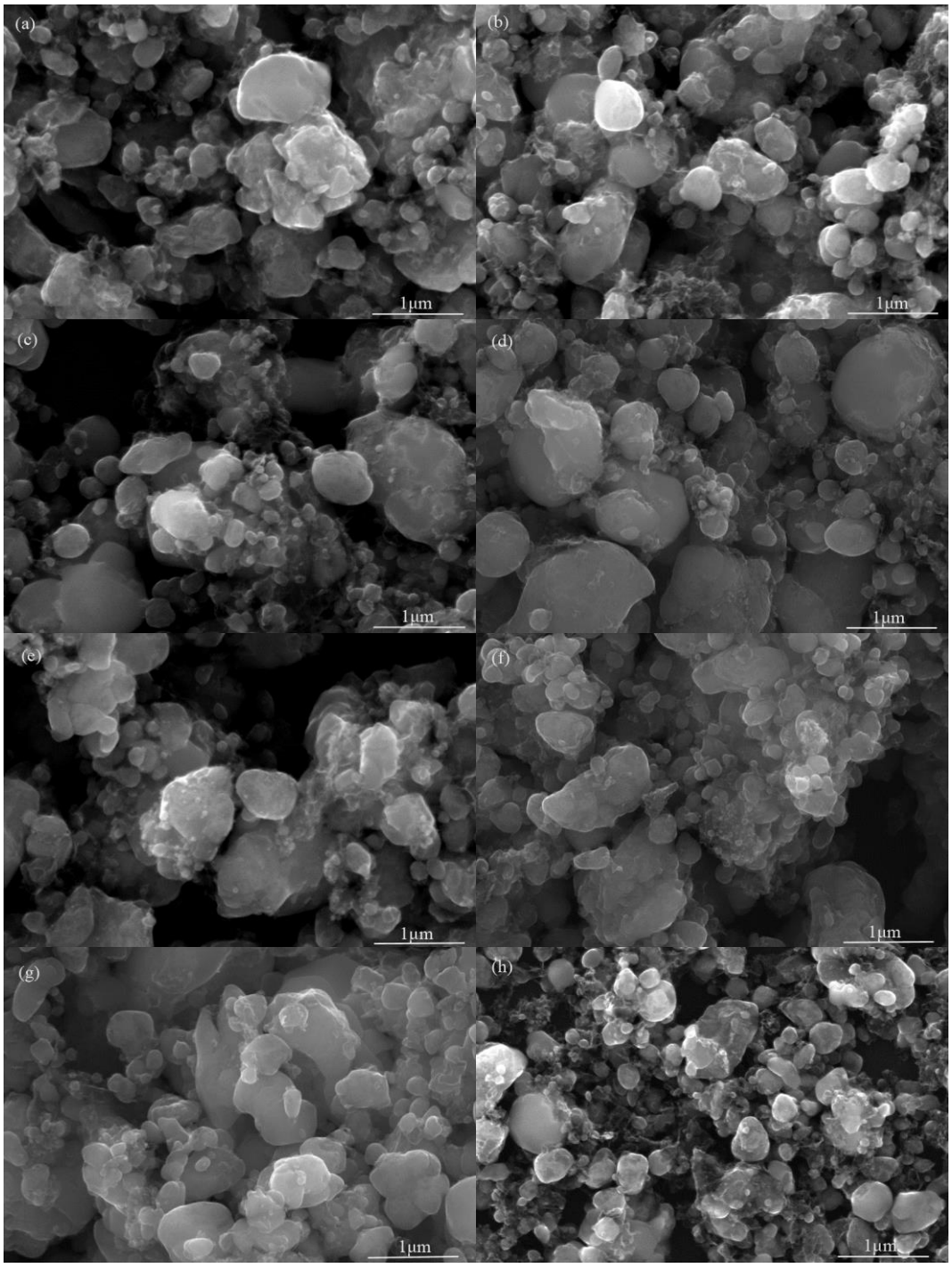

Figure 6. SEM images of $LiFePO_4$/C synthesized from $FePO_4$ obtained at different dehydration temperatures: (a) S200, (b) S300, (c) S400, (d) S450, (e) S500, (f) S600, (g) S700, (h) S500'.

Fig. 6 shows SEM images of $LiFePO_4$/C synthesized from $FePO_4$ obtained at different dehydration temperatures. Although the $FePO_4$ obtained at different dehydration temperatures has

apparent difference in particle size and morphology, no significant difference is observed on the prepared $LiFePO_4$/C powders. This phenomenon is associated with the wet ball milling process for raw materials mixing which eliminates the most difference in particle size and morphology of the $FePO_4$ obtained at different dehydration temperatures. In addition, increasing solid/liquid ratio and extending ball-milling time can further reduce the size of $LiFePO_4$/C particles as compared Fig. 6e with Fig. 6h.

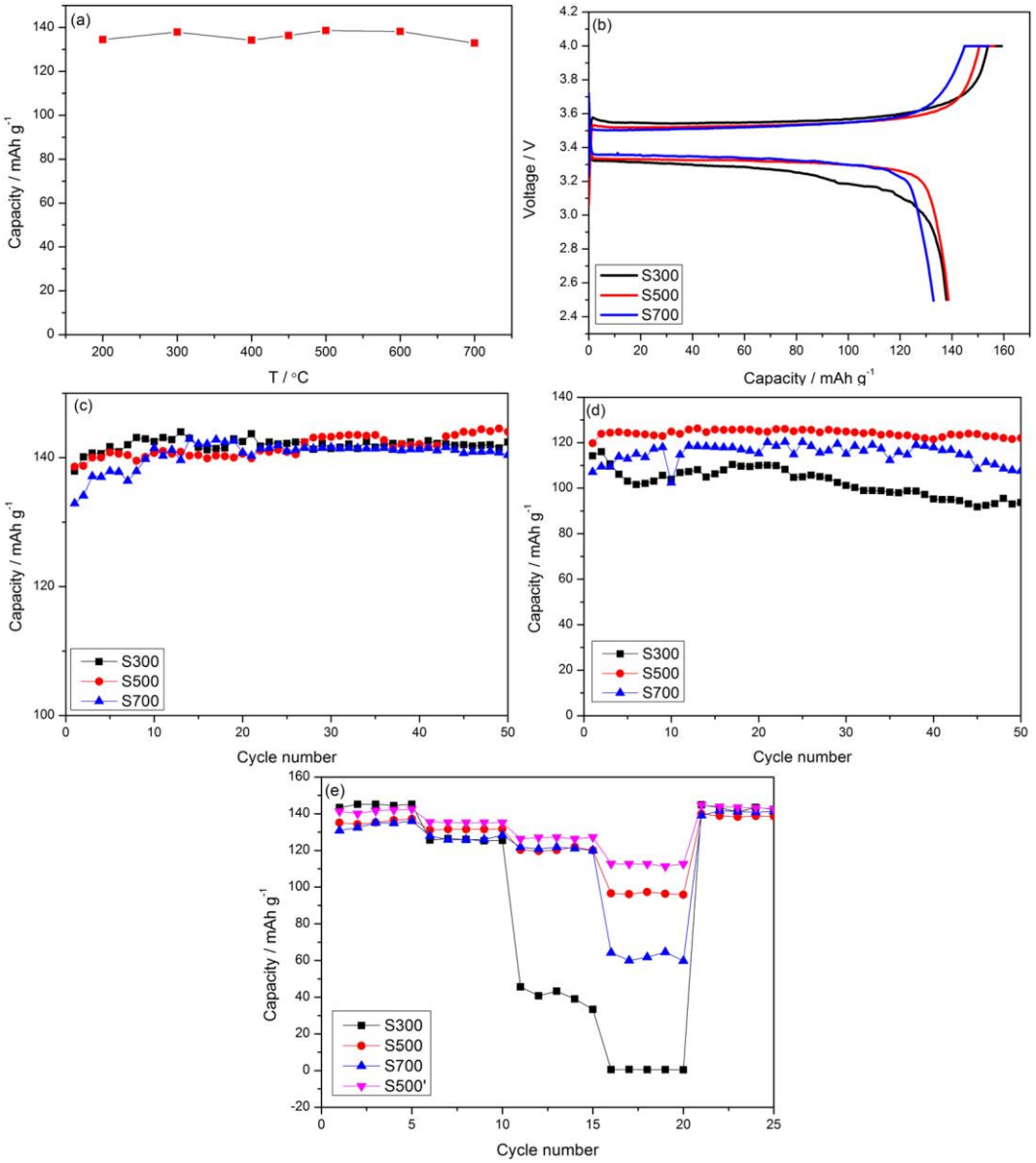

Figure 7. (a) The initial discharge capacity of $LiFePO_4$/C synthesized from $FePO_4$ obtained at different dehydration temperatures at 0.2 C. (b) Initial charge/discharge curves of the $LiFePO_4$/C at 0.2 C. (c) and (d) Cycling performance of $LiFePO_4$/C at 0.2 C and 1 C, respectively. (e) Rate performance of $LiFePO_4$/C.

Fig. 7 presents electrochemical performance of $LiFePO_4$/C synthesized from $FePO_4$ obtained at different dehydration temperatures. As shown in Fig. 7a, the initial discharge capacity of S200, S300, S400, S450，S500, S600 and S700 samples at the rate of 0.2 C is 134.5, 137.9, 134.2, 136.3, 138.6, 138.2, 137.8 and 132.9 mAh g^{-1}, respectively. Clearly, the difference in capacity cycled at a low rate is

not significant between samples. Especially in the subsequent cycles, the difference in discharge capacity becomes smaller gradually. For succinctness, only representative data are shown in other figures (Fig. 7b-e). It is seen that there is only a marginal difference in discharge capacity between samples after ten cycles as shown in Fig. 9c. The initial charge/discharge curves of S300, S500 and S700 at 0.2 C are shown in Fig. 7b. Although all samples exhibit a similar curve profile with voltage plateaus at ~3.4 V, a relatively larger polarization is observed on the sample of S300, indicating that this sample has a higher resistance. Therefore, when the cycling rate was raised up to a moderate rate of 1 C, the difference in discharge capacity becomes obvious. As compared with the samples (S200, S300, S400, S700) synthesized from $FePO_4$ obtained at lower or higher dehydration temperatures, the samples (S500 and S600) synthesized from $FePO_4$ obtained at moderate dehydration temperatures deliver higher capacity and have better cycling stability. Fig. 7d shows the representative data of S300, S500 and S700 samples. At higher rates, the difference in capacity becomes more obvious. Fig. 7e shows the rate performance of S300, S500 and S700 samples. The sample of S500 has the best rate performance and can deliver a capacity of ~96 mAh g^{-1} at 2 C which is much higher than that of S300 and S700 samples.

On the whole, the capacity of all samples is not high especially at high rates mainly due to the relatively large primary particle size of $LiFePO_4$/C. From previous reports [20, 23, 24], the performance of $LiFePO_4$ can be effectively improved by reducing its particle size. In this work, smaller primary particles of $LiFePO_4$/C (S500') could be obtained by decreasing liquid/solid ratio and extending ball-milling time for raw materials mixing as shown in Fig. 7h, and consequently the electrochemical performance at high rates of $LiFePO_4$/C was highly improved as shown in Fig. 7e, and the discharge capacity at 2 C can be largely increased from 96 to 112.7 mAh g^{-1}. Since the particle size distribution is not homogeneous and there still exists some big particles in the sample as shown in Fig. 7h, which is detrimental to utilization of the materials as pointed out by Newman et al. [25], the performance of this sample (S500') is still not so high as compared to those summarized by Zhang [26], but it is noted that the loading of active material in the cathode in this work is much higher than those reported in most previous literature. In light of the report by Yu et al. [27], a higher loading of active material in the cathode will result in a rapid decrease in capacity at high rates. In this respect, the performance of the sample (S500') is excellent at a high loading of active material despite the presence of big particles. This may be associated with the use of α-quartz $FePO_4$ as a raw material for synthesis of $LiFePO_4$/C. Moreover, it is expected that the performance can be further improved by tailoring particle size and carbon coating through optimization of materials preparation and processing, which is beyond the scope of the present work.

From the above results, it is seen that the dehydration temperature has an apparent influence on the crystalline form, particle size and morphology of $FePO_4$, and the difference in particle size and morphology of the $FePO_4$ obtained at different dehydration temperatures can be almost eliminated by subsequent wet ball milling process for raw materials mixing, but $LiFePO_4$/C composites synthesized from these $FePO_4$ still exhibit different electrochemical performance. These observations suggest that the crystalline form of $FePO_4$ exerts certain influence on the electrochemical performance of $LiFePO_4$/C, and the α-quartz $FePO_4$ with a trigonal structure ($P3_121$) is a more favorable form for better synthesis of $LiFePO_4$/C composite. Such an effect was not considered in the past, but the present

study suggests that particle size and crystalline form of $FePO_4$ should be considered at the same time. From our measurement (Fig. 3) and the available literature [9, 13, 15], it is known that the formation of α-quartz $FePO_4$ starts around 450 ^oC, and undesirable particle growth of $FePO_4$ has started at the dehydration temperature of 500 ^oC (Fig. 4f) and becomes severe at the dehydration temperature of 600 ^oC (Fig. 4g), which is detrimental to the efficient synthesis of small size $LiFePO_4$/C composite. Although large particles of $FePO_4$ can be broken into small particles by subsequent processing such as sufficient wet ball milling (4h) for raw materials mixing in this work, it will reduce production efficiency and raise processing cost. Therefore, to obtain α-quartz $FePO_4$ with small particle size for efficient synthesis of $LiFePO_4$/C composite with good electrochemical performance, the dehydration of $FePO_4 \cdot 2H_2O$ is proposed to be controlled at ~ 500 ^oC.

4. CONCLUSION

$FePO_4 \cdot 2H_2O$ can be completely dehydrated at a temperature above 184 ^oC, and the $FePO_4$ obtained at different dehydration temperatures has different crystalline form, particle size and morphology. $LiFePO_4$/C composites synthesized from these $FePO_4$ have similar crystallinity, particle size and morphology, but exhibit different electrochemical performance. The results suggest that the crystalline form of $FePO_4$ has a certain influence on the electrochemical performance of $LiFePO_4$/C, and the α-quartz $FePO_4$ with a trigonal structure (*$P3_121$*) is demonstrated to be an optimum form. To obtain small α-quartz $FePO_4$ particles for efficient synthesis of high performance $LiFePO_4$/C composite, it is proposed that the dehydration temperature should be controlled at ~ 500 ^oC.

ACKNOWLEDGEMENTS
This work is supported by the National Natural Science Foundation of China [grant numbers 51664031 and 51304098].

References

1. A.K. Padhi, K.S. Nanjundaswamy, and J.B. Goodenough, *J. Electrochem. Soc.*, 144 (1997) 1188.
2. J. Liu, Z. Wang, G. Zhang, Y. Liu, and A. Yu, *Int. J. Electrochem. Sci.*, 8 (2013) 2378.
3. X. Yang, J. Tu, M. Lei, Z. Zuo, B. Wu, and H. Zhou, *Electrochim. Acta*, 193 (2016) 206.
4. J. Liu, J. Wang, X. Yan, X. Zhang, G. Yang, A.F. Jalbout, and R. Wang, *Electrochim. Acta*, 54 (2009) 5656.
5. K. Yang, Z. Deng, and J. Suo, *J. Power Sources*, 201 (2012) 274.
6. F. Gao, Z. Tang, and J. Xue, *Electrochim. Acta*, 53 (2007) 1939.
7. F. Yu, J. Zhang, Y. Yang, and G. Song, *Electrochim. Acta*, 195 (2010) 6873.
8. S.E. Park, J.S. Chang, Y.K. Hwang, D.S. Kim, S.H. Jhung, and J.S. Hwang, *CrystEngComm*, 16 (2014) 2818.
9. P. Reale, and B. Scrosati, *Chem. Mater.*, 15 (2003) 5051.
10. Y. Zhu, Z. Ruan, S. Tang, and V. Thangadurai, *Ionic*s, 20 (2014) 1501.
11. S. Scaccia, M. Carewska, A.D. Bartolomeo, and P.P. Prosini, *Thermochim. Acta*, 397 (2003) 135.
12. K. Zaghib, and C.M. Julien, *J. Power Sources*, 142 (2005) 279.
13. B. Boonchom, and S. Puttawon, *Physica B*, 405 (2010) 2350.
14. K. Taxer, and H. Bartl, *Cryst. Res. Technol.*, 12 (2004) 1080.

15. Y. Song, P.Y. Zavalij, M. Suzuki, and M.S. Whittingham, *Inorg. Chem.*, 41 (2002) 5778.
16. L. Wang, G. Liang, X. Ou, X. Zhi, J. Zhang, and J. Cui, *J. Power Sources*, 189 (2009) 423.
17. C. Mi, X. Zhao, G. Cao, and J. Tu, *J. Electrochem. Soc.*, 152 (2005) A483.
18. Y. Lv, Y. Long, J. Su, X. Lv, and Y. Wen, *Electrochim. Acta*, 119 (2014) 155.
19. J. Ren, W. Pu, X. He, C. Jiang, and C. Wan, *Ionics*, 17 (2011) 581.
20. C. Delacourt, P. Poizot, S. Levasseur, and C. Masquelier, *Electrochem. Solid-State Lett.*, 9 (2006) A352.
21. C.M. Burba, J.M. Palmer, and B.S. Holinsworth, *J.Raman Spectrosc*, 40(2009)225.
22. N. Aliouane, T. Badeche, Y. Gagou, E. Nigrelli, and P. Saint-Gregoire, *Ferroelectrics*, 241 (2000) 255.
23. A. Yamada, S.C. Chung, and K. Hinokuma, *J. Electrochem. Soc.*, 148 (2001) A224.
24. M. Gaberscek, R. Dominko, and J. Jamnik, *Electrochem. Commun.*, 9 (2007) 2778.
25. K. Striebel, J. Shim, V. Srinivasan, and J. Newman, *J. Electrochem. Soc.*, 152 (2005) A664.
26. W.J. Zhang, *J. Electrochem. Soc.*, 157 (2010) A1040.
27. D.Y.W. Yu, K. Donoue, T. Inoue, M. Fujimoto, and S. Fujitani, *J. Electrochem. Soc.*, 153 (2006) A835.